PCCP

Cite this: *Phys. Chem. Chem. Phys.*, 2011, **13**, 8985–8992

www.rsc.org/pccp

PAPER

Molecular engineering and theoretical investigation of organic sensitizers based on indoline dyes for quasi-solid state dye-sensitized solar cells

Bo Liu,*[a] Wenjun Wu,[b] Xiaoyan Li,[a] Lei Li,[c] Shaofu Guo,[a] Xiaoru Wei,[a] Weihong Zhu[b] and Qingbin Liu*[a]

Received 23rd February 2011, Accepted 3rd March 2011
DOI: 10.1039/c1cp20484j

Novel indoline dyes, **I-1**–**I-4**, with structural modification of π-linker group in the D-π-A system have been synthesized and fully characterized. Molecular engineering through expanding the π-linker segment has been performed. The ground and excited state properties of the dyes have been studied by means of density functional theory (DFT) and time-dependent DFT (TD-DFT). Larger π-conjugation linkers would lead to broader spectral response and higher molar extinction coefficient but would decrease dye-loaded amount on TiO_2 electrode and LUMO level. While applied in DSSCs, the variation trends in short-circuit current density (J_{sc}) and open-circuit voltage (V_{oc}) were observed to be opposite to each other. The internal reasons were studied by experimental data and theoretical calculations in detail. Notably, **I-2** showed comparable photocurrent values with liquid and quasi-solid state electrolyte, which suggested through molecular engineering of organic sensitizers the dilemma between optical absorption and charge diffusion lengths can be balanced well. Through studies of photophysical, electrochemical, and theoretical calculation results, the internal relations between chemical structure and efficiency have been revealed, which serve to enhance our knowledge regarding design and optimization of new sensitizers for quasi-solid state DSSCs, providing a powerful strategy for prediction of photovoltaic performances.

Introduction

Dye-sensitized solar cells (DSSCs), as promising candidate for solar-energy conversion device, has attracted considerable attention due to their high performance and low-cost of production.[1–3] As the critical component of DSSCs, sensitizers including ruthenium and metal-free organic dyes have been intensively investigated in recent years. The classic ruthenium complexes give a solar-to-electrical energy conversion efficiency of up to 11% under AM 1.5 irradiation with long time stability.[4,5] Through molecular design, several ruthenium derivatives, such as black dye,[6] Z907,[7] and K19,[8] also gained remarkable efficiency over 7%. However, the use of rare metals with heavy purification brings major problems in cost and environmental issues. Therefore, metal-free organic sensitizers, such as indoline,[9–12] fluorine,[13] triphenylamine,[14–17] coumarin,[18,19] and porphyrin[20] have been extensively explored and their performances characterized.

Most organic sensitizers are based on the D-π-A system. Among donor groups, indoline, possessing strong light-capturing and electron-donating capabilities, is an excellent candidate. Some sensitizers containing an indoline group as donor have been synthesized and show very promising results. Uchida *et al.* combined indoline derivatives with rhodanine ring and obtained a series of dyes, which presented a relatively broad action spectrum and high conversion efficiency up to 6.1%.[9] Through optimization of DSSCs devices, the conversion efficiencies using AcAN- and ionic-liquid-based electrolytes were enhanced to 9.03% and 6.67%, respectively.[10] Recently, we have also reported an indoline-based sensitizer. Using a 5.0 μm TiO_2 electrode, 7.41% conversion efficiency was obtained while N719 produced 7.03% under the same conditions.[11] However, there is still much room for further insight into interfacial engineering through molecular engineering.

As we all know, the π-linker segment can not only affect absorption spectra but also tune the HOMO and LUMO levels and some other properties. However, the efficiency is not always enhanced along with the expansion of π-conjugation system. This phenomenon has been reported by several groups but the understanding of the origins of such results is still limited.[15,16,18] Therefore, we can investigate the contributions of different π-linker and build spectral response and energy level libraries by alternating different π-linker segments. This screening

[a] *College of Chemistry and Material Science, Hebei Normal University, 113 East Yuhua Road, Shijiazhuang, Hebei, 050016, P. R. China. E-mail: liubo@mail.hebtu.edu.cn, qbinliu@yahoo.com; Tel: +86-311-86268311*
[b] *Key Laboratory of Advanced Material, Institute of Fine Chemicals, East China University of Science &Technology, 130 Meilong Road, Shanghai, 200237, P. R. China*
[c] *China National Petroleum Corporation Occupational Health Center, 51 Xinkai Road, Langfang, Hebei, 065000, P. R. China*

strategy helps us to optimize the TiO_2-sensitizer-hole transport material (HTM) system in terms of balance between spectral response, driving forces, and photovoltaic performance for future preparation of high efficiency dyes by matching suitable π-linker groups in the D-π-A system.[21] As the most developed group, triphenylamine was used as donor group for a series of dyes which were designed and synthesized by Sun *et al.* and the energy levels were tuned efficiently.[14] However, we can not apply previous experiences to guide works on novel systems directly due to their own characteristics of different functional groups. With this in mind, we have introduced thiophene into the framework to extend the conjugate system of dyes and developed a series of dyes based on indoline group. The chemical structures of new dyes were confirmed by ^{1}H NMR, ^{13}C NMR, and HR-MS. The DSSC devices based on liquid and ionic liquid electrolytes have been fabricated. The absorption spectra, dye-loaded amounts, energy levels, and photovoltaic performances were tuned and studied in detail. Through these studies, the internal relations between chemical structure and efficiency have been revealed, which serve to enhance our knowledge regarding design and optimization of new sensitizers for quasi-solid state DSSCs, providing a powerful strategy for prediction of photovoltaic performances.

Experimental

General

The FTO conducting glass (fluorine doped SnO_2, sheet resistance $< 15\ \Omega$/square, transmission $> 90\%$ in the visible) was obtained from Geao Science and Educational Co. Ltd., China. Titanium (IV) isopropoxide, lithium iodide, and *tert*-butylpyridine (TBP) were purchased from Aldrich. All other solvents and chemicals used were produced by Sinopharm Chemical Reagent Co., Ltd, China (reagent grade) and used as received. ^{1}H NMR spectra were obtained with a Bruker AM-400 spectrometer. The mass spectra were conducted on a 4700 Proteomics Analyzer spectrometer.

Physical measurements

UV-visible spectra were determined with a Varian Cary 500 spectrometer. Fluorescent spectra were recorded on a Varian Cary Eclipse spectrometer. The cyclic voltammograms were measured on a Versastat II electrochemical workstation (Princeton Applied Research) using a normal three-electrode cell with a dye-loaded TiO_2 electrode as working electrode, a Pt wire auxiliary electrode, a Ag/AgCl reference electrode in saturated KCl solution, and 0.1 M tetrabutylammonium hexafluorophosphoric acid was used as supporting electrolyte. After the measurement, ferrocene was added as the internal reference for calibration.

Fabrication and measurement of solar cells

A screen-printed double layer of TiO_2 particles was used as photoelectrode. A 10 mm thick film of 13 nm sized TiO_2 particles (Ti-Nanoxide T/SP) was first printed on the FTO conducting glass and further coated with a 4 mm thick second layer of 400 nm light-scattering anatase particles (Ti-Nanoxide 300). Sintering was carried out at 450 °C for 30 min. Before immersion in the dye solution, these films were immersed in a 40 mM aqueous $TiCl_4$ solution at 70 °C for 30 min and washed with water and ethanol. Then the films were heated again at 450 °C for 30 min followed by cooling to 80 °C and dipping into a 3×10^{-4} M solution of dye in acetonitrile for 12 h at room temperature. To prepare the counter electrode, the Pt catalyst was deposited on the cleaned FTO glass by coating with a drop of H_2PtCl_6 solution (0.02 M in 2-propanol solution) with heat treatment at 400 °C for 15 min. A hole (0.8 mm diameter) was drilled on the counter electrode using a drill-press. The perforated sheet was cleaned with ultrasound in an ethanol bath for 10 min. For the assembly of DSSCs, the dye-loaded TiO_2 electrode and Pt-counter electrode were assembled into a sandwich type cell and sealed with a hot-melt gasket of 25 mm thickness made of the ionomer Surlyn 1702 (DuPont). The size of the TiO_2 electrodes used was 0.25 cm^2 (*i.e.* 5 mm × 5 mm). A drop of the electrolyte was put on the hole in the back of the counter electrode. It was introduced into the cell *via* vacuum backfilling. The hole in the counter electrode was sealed with a film of Surlyn 1702 and a cover glass (0.1 mm thickness) using a hot iron bar.

The electrolyte employed was a solution of 0.6 M PMII (1-propyl-3-methylimidazolium iodide), 0.05 M I_2, 0.10 M LiI and 0.5 M 4-*tert*-butylpyridine in a mixture of acetonitrile and methoxypropionitrile (v/v, 7 : 3). The quasi-solid state electrolyte consisted of 1-butyl-3-methylimidazolium iodide (BMII)/I_2/benzimidazole (BI)/GuSCN (w/w, 40/1.67/0.67/3.33).

Photovoltaic measurements employed an AM 1.5 solar simulator equipped with a 300 W xenon lamp (Model No. 91160, Oriel). The power of the simulated light was calibrated to 100 mW cm^{-2} using a Newport Oriel PV reference cell system (Model 91150V). *I–V* curves were obtained by applying an external bias to the cell and measuring the generated photocurrent with a Keithley model 2400 digital source meter. The voltage step and delay time of photocurrent were 10 mV and 40 ms, respectively. The cell active area was tested with a mask of 0.158 cm^2. The photocurrent action spectra were measured with an IPCE test system consisting of a Model SR830 DSP Lock-In Amplifier and a Model SR540 Optical Chopper (Stanford Research Corporation, USA), a 7IL/PX150 xenon lamp and power supply, and a 7ISW301 Spectrometer. Each value in this paper was an average of three samples.

Synthesis

The chemical structures and synthetic routes of **I-1**–**I-4** were shown in Scheme 1 as well as all the intermediates (compound **1**–**9**).

***Trans*-2-cyano-3-(4-p-tolyl-1,2,3,3a,4,8b-hexahydrocyclopenta-[b]indol-7-yl)acrylic acid (I-1).** A 30 mL acetonitrile solution of **1** (0.277 g, 1 mmol), cyanoacetic acid (0.11 g, 1.3 mmol), and piperidine (0.1 g, 1.2 mmol) was refluxed for 6 h under nitrogen atmosphere. The resultant mixture was poured into 0.1 M HCl solution (100 mL). The product was filtered and recrystallized in DCM/petroleum ether. **I-1** was obtained as a dark purple solid (0.26 g, 76%). ^{1}H NMR (500 MHz, DMSO) δ ppm: 13.3 (s, 1H), 8.05 (s, 1H), 7.92 (s, 1H), 7.70–7.72 (m, 1H), 7.24–7.29 (m, 4H), 6.75 (d, J = 8.5 Hz, 1H), 5.04 (t, J = 8.5 Hz, 1H),

3.84 (t, J = 8.5 Hz, 1H), 2.32 (s, 3H), 2.01–2.10 (m, 1H), 1.60–1.78 (m, 4H), 1.32–1.41 (m, 1H). ^{13}C NMR (125 MHz, DMSO) δ ppm: 165.2, 154.0, 153.1, 137.8, 136.4, 135.5, 134.2, 130.5, 127.2, 122.5, 121.7, 118.4, 106.7, 94.2, 69.8, 44.3, 35.6, 32.9, 24.2, 21.0. HR-MS (TOF MS ES+) m/z 345.1605 [M + H$^+$] calcd for $C_{22}H_{21}N_2O_2$ (M + H$^+$) 345.1603.

5-(4-p-tolyl-1,2,3,3a,4,8b-hexahydrocyclopenta[b]indol-7-yl)-thiophene-2-carbaldehyde (4). A 15 mL THF solution of **2** (0.328 g, 1 mmol), **3** (0.156 g, 1 mmol), Pd(PPh$_3$)$_4$ (0.1 g, ~0.1 mmol), and 2 M Na_2CO_3 (5 mL) was refluxed for 24 h under nitrogen atmosphere. The resultant mixture was poured into 50 mL water and extracted with CH_2Cl_2 (3 × 30 mL). The combined organic extract was dried over anhydrous Na_2SO_4 and filtered. Solvent removal by rotary evaporation and column chromatography over silica gel with a petroleum ether/ethyl acetate mixture (20 : 1) was followed by recrystallizing in DCM/petroleum ether. Product **4** was obtained as a yellow solid (0.19 g, 53%). ^{1}H NMR (500 MHz, $CDCl_3$) δ ppm: 9.81 (s, 1H), 7.67 (d, J = 4.0 Hz, 1H), 7.40 (s, 1H), 7.36–7.38 (m, 1H), 7.23 (d, J = 4.0 Hz, 1H), 7.16–7.19 (m, 4H), 6.83 (d, J = 8.5 Hz, 1H), 4.84 (t, J = 8.5 Hz, 1H), 3.84 (t, J = 8.5 Hz, 1H), 2.34 (s, 3H), 2.03–2.12 (m, 1H), 1.87–1.94 (m, 2H), 1.65–1.71 (m, 2H), 1.51–1.62 (m, 1H).

***Trans*-2-cyano-3-(5-(4-p-tolyl-1,2,3,3a,4,8b-hexahydrocyclopenta[b]indol-7-yl)thiophen-2-yl)acrylic acid (I-2).** A 30 mL acetonitrile solution of **4** (0.359 g, 1 mmol), cyanoacetic acid (0.11 g, 1.3 mmol), and piperidine (0.1 g, 1.2 mmol) was refluxed for 6 h under nitrogen atmosphere. The resultant mixture was poured into 0.1 M HCl solution (100 mL). The product was filtered and recrystallized in DCM/petroleum ether. **I-2** was obtained as a dark purple solid (0.33 g, 78%). ^{1}H NMR (500 MHz, DMSO) δ ppm: 8.35 (s, 1H), 7.88 (d, J = 4.0 Hz, 1H), 7.54–7.55 (m, 2H), 7.45 (s, 1H), 7.20–7.24 (m, 4H), 6.83 (d, J = 8.5 Hz, 1H), 4.93 (t, J = 8.5 Hz, 1H), 3.86 (t, J = 8.5 Hz, 1H), 2.30 (s, 3H), 2.03–2.11 (m, 1H), 1.62–1.83 (m, 4H), 1.35–1.44 (m, 1H). ^{13}C NMR (125 MHz, DMSO) δ ppm: 164.6, 154.7, 149.4, 145.8, 141.6, 139.3, 136.4, 132.8, 132.2, 130.4, 126.9, 123.0, 122.8, 122.7, 121.0, 117.9, 107.4, 69.1, 44.8, 35.4, 33.4, 24.4, 20.9. HR-MS (TOF MS ES+) m/z 427.1479 [M + H$^+$] calcd for $C_{26}H_{22}N_2O_2S$ (M + H$^+$) 427.1480.

***Trans*-7-(2-(thiophen-2-yl)vinyl)-4-p-tolyl-1,2,3,3a,4,8b-hexahydrocyclopenta[b]indole (6). 5** (0.439 g, 1 mmol) was dispersed in 15 mL dry THF followed by the addition of NaH (0.03 g, 1.25 mmol). The mixture was stirred at ambient temperature under nitrogen atmosphere for 1 h. I-CHO (0.277 g, 1 mmol) was added and the reaction mixture was allowed to stir at ambient temperature for another 48 h. Then the mixture was poured into 100 mL HCl solution (0.1 M) and extracted with DCM. The organic phase was dried over Na_2SO_4, then filtered through a plug of silica gel with petroleum ether/ethyl acetic mixture (100 : 1), and a crude intermediate was obtained as a mixture of isomers. The crude product **6** was used directly in the next step without further purification.

***Trans*-5-(2-(4-p-tolyl-1,2,3,3a,4,8b-hexahydrocyclopenta[b]-indol-7-yl)vinyl)thiophene-2-carbaldehyde (7). 6** was dissolved in THF (10 mL) and the solution was cooled to −78 °C under nitrogen atmosphere. *N*-Butyl lithium (0.8 mL, 2.2 M hexane solution) was added dropwise over 5 min and the mixture was stirred at −78 °C for 1 h. Then the mixture was allowed to warm to 0° C and stirred for 30 min. The mixture was once again cooled to −78° C and DMF (0.1 mL, 1.3 mmol) was added. The reaction was allowed to warm to ambient temperature and was stirred for 2 h. The reaction was quenched by the addition of 0.5 M HCl (100 mL) and extracted with DCM. After drying over Na_2SO_4, the combined organic extract was concentrated by rotary evaporation and column chromatography over silica gel with petroleum ether/ethyl acetic mixture (20 : 1). The *trans*-type isomer **7** was obtained as a red solid (0.22 g, 58%). ^{1}H NMR (500 MHz, $CDCl_3$) δ ppm: 9.81 (s, 1H), 7.62 (d, J = 4.0 Hz, 1H), 7.30 (s, 1H), 7.14–7.17 (m, 5H), 7.08 (d, J = 16.0 Hz, 1H), 7.04 (J = 4.0 Hz, 1H), 6.99 (d, J = 16.0 Hz, 1H), 6.81 (d, J = 8.5 Hz, 1H), 4.82 (t, J = 8.5 Hz, 1H), 3.81 (t, J = 8.5 Hz, 1H), 2.34 (s, 3H), 2.01-2.10 (m, 1H), 1.85–1.93 (m, 2H), 1.49–1.79 (m, 3H).

***Trans*-2-cyano-3-(5-((E)-2-(4-p-tolyl-1,2,3,3a,4,8b-hexahydrocyclopenta[b]indol-7-yl)vinyl)thiophen-2-yl)acrylic acid (I-3).** A 30 mL acetonitrile solution of **7** (0.2 g, 0.52 mmol), cyanoacetic acid (0.11 g, 1.3 mmol), and piperidine (0.1 g, 1.2 mmol) was refluxed for 6 h under nitrogen atmosphere. The resultant mixture was poured into 100 mL HCl solution (0.1 M). The product was filtered and recrystallized in DCM/petroleum ether. I-3 was obtained as a dark purple solid (0.18 g, 78%). ^{1}H NMR (500 MHz, DMSO) δ ppm: 8.20 (s, 1H), 6.67 (d, J = 4.0 Hz, 1H), 7.46 (s, 1H), 7.16–7.28 (m, 7H), 7.03 (d, J = 16.0 Hz, 1H), 6.79 (d, J = 8.5 Hz, 1H), 4.86 (t, J = 8.5 Hz, 1H), 3.79 (t, J = 8.5 Hz, 1H), 2.28 (s, 3H), 1.95–2.08 (m, 1H), 1.65–1.82 (m, 4H), 1.28–1.40 (m, 1H). ^{13}C NMR (125 MHz, DMSO) δ ppm: 165.0, 150.6, 148.3, 142.6, 139.7, 137.9, 136.0, 134.4, 132.3, 131.5, 130.2, 128.5, 127.0, 126.1, 123.1, 120.3, 119.2, 118.7, 117.0, 107.2, 68.8, 44.9, 35.2, 33.5, 24.4, 20.9. HR-MS (TOF MS ES+) m/z 453.1634 [M + H$^+$] calcd for $C_{28}H_{25}N_2O_2S$ (M + H$^+$) 453.1637.

***Trans*-7-(5-(2-(thiophen-2-yl)vinyl)thiophen-2-yl)-4-p-tolyl-1,2-,3,3a,4,8b-hexahydrocyclopenta[b]indole (8). 5** (0.439 g, 1 mmol) was dispersed in 15 mL dry THF followed by the addition of NaH (0.03 g, 1.25 mmol). The mixture was stirred at ambient temperature under nitrogen atmosphere for 1 h. **4** (0.359 g, 1 mmol) was added and the reaction mixture was allowed to stir at ambient temperature for another 48 h. Then the mixture was poured into 100 mL HCl solution (0.1 M) and extracted with DCM. The organic phase was dried over Na_2SO_4, then filtered through a plug of silica gel with petroleum ether/ethyl acetic mixture (100 : 1), and a crude intermediate was obtained as a mixture of isomers. The crude product **8** was used directly in the next step without further purification.

***Trans*-5-(2-(5-(4-p-tolyl-1,2,3,3a,4,8b-hexahydrocyclopenta-[b]-indol-7-yl)thiophen-2-yl)vinyl)thiophene-2-carbaldehyde (9). 8** was dissolved in THF (10 mL) and the solution was cooled to −78 °C under nitrogen atmosphere. *N*-Butyl lithium (0.8 mL, 2.2 M hexane solution) was added dropwise over 5 min and the mixture was stirred at −78 °C for 1 h. Then the mixture was allowed to warm to 0 °C and was stirred for 30 min. The mixture was once again cooled to −78 °C and DMF (0.1 mL, 1.3 mmol)

was added. The reaction was allowed to warm to ambient temperature and was stirred for 2 h. The reaction was quenched by the addition of 0.5 M HCl (100 mL) and extracted with DCM. After drying over Na_2SO_4, the combined organic extract was concentrated by rotary evaporation and column chromatography over silica gel with petroleum ether/ethyl acetic mixture (15 : 1). The *trans*-type isomer **9** was obtained as a red solid (0.20 g, 43%). ^{1}H NMR (500 MHz, $CDCl_3$) δ ppm: 9.83 (s, 1H), 7.63 (d, J = 4.0 Hz, 1H), 7.34 (s, 1H), 7.28–7.30 (m, 1H), 7.22 (d, J = 16.0 Hz, 1H), 7.15–7.19 (m, 4H), 7.05–7.78 (m, 3H), 6.93 (d, J = 16.0 Hz, 1H), 6.85 (d, J = 8.0 Hz, 1H), 4.81 (t, J = 8.5 Hz, 1H), 3.84 (t, J = 8.5 Hz, 1H), 2.34 (s, 3H), 2.03–2.11 (m, 1H), 1.87–1.93 (m, 2H), 1.75–1.83 (m, 1H), 1.64–1.70 (m, 1H), 1.51–1.59 (m, 1H).

***Trans*-2-cyano-3-(5-(*trans*-2-(5-(4-p-tolyl-1,2,3,3a,4,8b-hexahydrocyclopenta[b]indol-7-yl)thiophen-2-yl)vinyl)thiophen-2-yl)-acrylic acid (I-4).** A 30 mL acetonitrile solution of **9** (0.467 g, 1 mmol), cyanoacetic acid (0.11 g, 1.3 mmol), and piperidine (0.1 g, 1.2 mmol) was refluxed for 6 h under nitrogen atmosphere. The resultant mixture was poured into 0.1 M HCl solution (100 mL). The product was filtered and recrystallized in DCM/petroleum ether. **I-4** was obtained as a dark purple solid (0.34 g, 64%). ^{1}H NMR (500 MHz, DMSO) δ ppm: 8.11 (s, 1H), 7.64 (d, J = 3.5 Hz, 1H), 7.43 (s, 1H), 7.27–7.31 (m, 5H), 7.17–7.22 (m, 4H), 7.10 (d, J = 16.0 Hz, 1H), 6.84 (d, J = 3.5 Hz, 1H), 4.87 (t, J = 8.5 Hz, 1H), 3.84 (t, J = 8.5 Hz, 1H), 2.29 (s, 3H), 2.01–2.09 (m, 1H), 1.69–1.83 (m, 3H), 1.58–1.65 (m, 1H), 1.34–1.43 (m, 1H). ^{13}C NMR (125 MHz, DMSO) δ ppm: 164.3, 148.2, 147.8, 145.4, 141.3, 139.9, 138.8, 136.9, 136.1, 135.7, 131.4, 130.6, 130.3, 127.4, 125.6, 124.8, 124.1, 122.5, 122.3, 120.2, 119.8, 119.6, 107.6, 68.8, 45.0, 35.2, 33.6, 24.4, 20.8. HR-MS (TOF MS ES+) m/z 535.1519 [M + H$^+$] calcd for $C_{32}H_{27}N_2O_2S_2$ (M + H$^+$) 535.1514.

Results and discussion

Synthesis

The chemical structures and synthetic routes of four dyes were shown in Scheme 1. In a typical D-π-A system, the indoline unit, whose preparation has been successfully scaled up to a hundred kilograms,[11] was applied as donor group. Cyanoacetic acid was used as the acceptor group. Thiophene is employed to provide conjugation between donor and acceptor groups. The Suzuki coupling reaction, Wittig reaction, and Knoevenagel reaction were applied in the synthetic routes. It is noteworthy that the synthesis of these dyes was quite straightforward and capable of scaling up since the important intermediates including indoline derivatives and 5-formyl-thiophene-2-boronic acid are commercially available.

Photophysical and electrochemical characterization

Fig. 1a showed the absorption and emission spectra of the dyes in THF. Absorption peaks were observed in the visible region at 438, 492, 504, and 518 nm, respectively. The λ_{max} was red-shifted from 438 nm to 518 nm as the π-conjugation expanded and the absorption spectra were broadened in visible region, which would obviously favor light harvesting in DSSCs. Also, the molar extinction coefficient was enhanced. The molar extinction coefficient at λ_{max} of **I-4** was determined to be 4.86×10^4 M^{-1} cm^{-1} at 518 nm, which is about 4 times the corresponding value of **I-1** (1.22×10^4 M^{-1} cm^{-1} at 438 nm) in the visible region (Table 1).

When anchored on TiO_2, absorption peaks of four dyes showed blue-shifts in different extents (Fig. 1b). Apparently, along with the broader spectra for **I-3** and **I-4**, the cells could be expected to exhibit better IPCE performances. Furthermore, after anchoring on TiO_2, the absorption threshold was red shifted. Take **I-2** for example, when adsorbed on TiO_2, the absorption threshold was red shifted by approximately 100 nm from 600 nm to 700 nm due to the interaction between the carboxylate group and TiO_2.[4]

To evaluate the possibility of electron transfer from the excited dye molecule to the conduction band (CB) of TiO_2, cyclic voltammograms were performed in acetonitrile. Table 2 summarizes their HOMO levels and the LUMO levels.

The LUMO levels of the dyes anchored on TiO_2 film lie in the order **I-1** < **I-2** < **I-3** < **I-4**, and were determined to be −1.43, −1.35, −1.30, and −1.26 V *vs.* NHE, respectively, which were more negative than the CB edge of TiO_2 (−0.5 V *vs.* NHE),

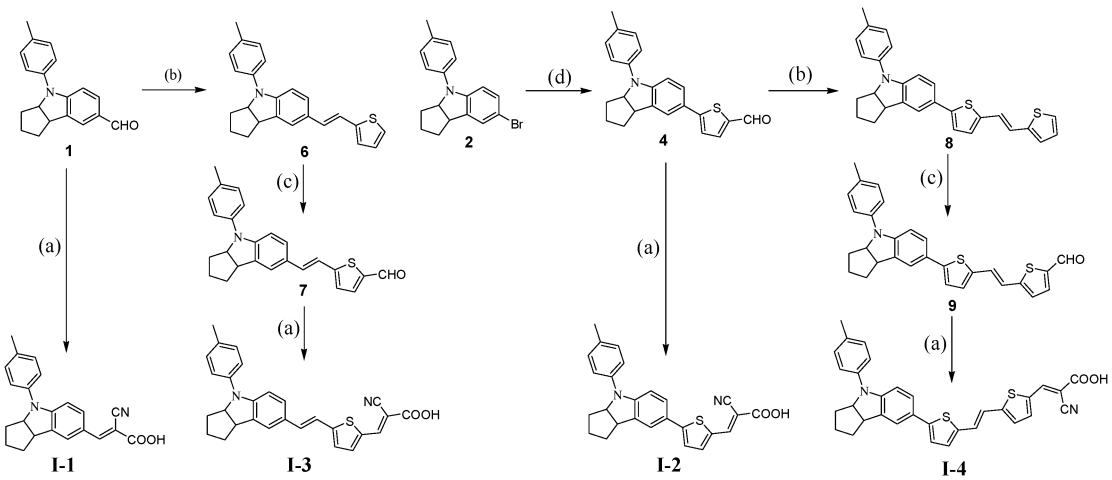

Scheme 1 Chemical structures and synthetic routes of indoline dyes (a) cyanoacetic acid, AcAN, reflux; (b) 2-PPh_3Br-methyl-thiophen (**5**), THF, NaH, rt; (c) $POCl_3$, DMF, reflux; (d) 5-formylthiophen-2-ylboronic acid (**3**), Na_2CO_3, $Pd(PPh_3)_4$, THF, reflux.

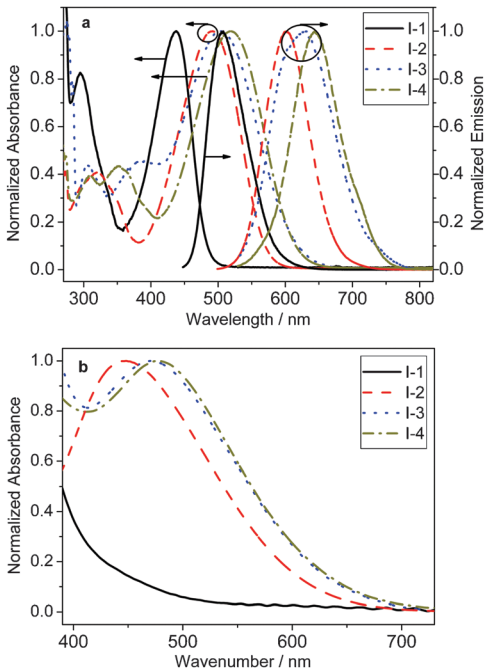

Fig. 1 Normalized absorbance and emission of dyes (a) in THF and (b) normalized absorbance on TiO_2 in visible region.

Table 1 Absorption and emission properties measured in THF and on TiO_2

	$\lambda_{max}{}^a$/nm	ε/M^{-1} cm^{-1}	E_{max}/nm	$\lambda_{max}{}^b$/nm	Amount^c
I-1	438	12 200	508	354	3.56
I-2	492	37 400	603	447	4.18
I-3	504	41 500	629	471	3.87
I-4	518	48 600	644	480	2.43

[a] Absorption of the dyes in THF solution. [b] Absorption of the dyes adsorbed on TiO_2. [c] The dye-loaded amount ($\times 10^{-7}$ mol cm^{-2}) was determined by desorbing the dye from surfaces of TiO_2 electrodes into NaOH solution and was analyzed by UV-visible spectrometer.

ensuring that the excited electron injection to the CB of TiO_2 was thermodynamically favorable. It is noteworthy that compared with **I-4**, **I-2** and **I-3** gained more negative LUMO levels. As expected, the higher LUMO level is preferable in that a larger gap between LUMO and the CB will result in a larger possibility of electronic injection into the CB of TiO_2. The orbital energies were also calculated by hybrid density functional theory (B3LYP) with the 6-31G* basis set as implemented in the Gaussian 03 program.[22] The calculated LUMO energies for **I-1**, **I-2**, **I-3** and **I-4** are −2.28, −1.90, −1.84, and −1.68 V (shown in Table 2 and Fig. 2), respectively, which lie in the same order with the experimental results. The energies were overestimated partially due to the neglect of solvation effect. Consequently, taking both the corresponding extinction coefficient and orbital levels into consideration, **I-2** and **I-3** could be expected to possess better photovoltaic performances to a certain extent compared with **I-1** and **I-4**.

Table 2 Electrochemical properties of dyes **I-1**, **I-2**, **I-3**, and **I-4**

	Experimental^a (V)			Calculated^c (V)		
	HOMO	$E_{0-0}{}^b$	LUMO	HOMO	E_{0-0}	LUMO
I-1	1.19	2.62	−1.43	1.04	3.32	−2.28
I-2	0.90	2.25	−1.35	0.71	2.61	−1.90
I-3	0.88	2.18	−1.30	0.66	2.50	−1.84
I-4	0.84	2.10	−1.26	0.44	2.12	−1.68

[a] Electrochemical properties of the dyes adsorbed on TiO_2 films. [b] E_{0-0} values were estimated from the intersection of normalized absorption and emission curves from solution measurements. [c] Calculated at the B3LYP/6-31G* level in vacuum.

TDDFT calculation (See Table 3) shows the lowest transition of charge transfer character from the donor moiety to the acceptor, which is favorable for the charge injection. The overestimates of the lowest transition energy for the dyes are related to the more extended charge-transfer nature of this transition.[23] This screening strategy helps us to optimize the TiO_2-sensitizer-HTM system in terms of balance between spectral response, driving forces, and photovoltaic performance for future preparation of high efficiency dyes by matching suitable π-linker groups in the D-π-A system.[14,21]

Photovoltaic performance evaluation

The IPCE action spectra of DSSCs sensitized by four dyes without light scattering layer on TiO_2 electrode are presented in Fig. 3, which matched well with the absorbance spectra of dye-loaded TiO_2 film. Due to poor absorption (Fig. 1b), **I-1** showed very low IPCE values in the visible region and decreased to zero at about 560 nm. **I-2** gained the highest IPCE value (84%) among four dyes at about 478 nm and exceeded 70% in the range of 415–525 nm.

Compared with **I-2**, **I-3** presented a slightly lower maximum IPCE value (77% at 480 nm), but the action region was much broader, that is, the threshold was red-shifted from 690 nm to about 740 nm. Therefore, the slightly higher short-circuit current density (J_{sc}) of **I-3** was reasonable. In the case of **I-4**, although it showed the broadest spectra, the values were relatively low, which led to the lower J_{sc} (6.13 mA cm^{-2}).

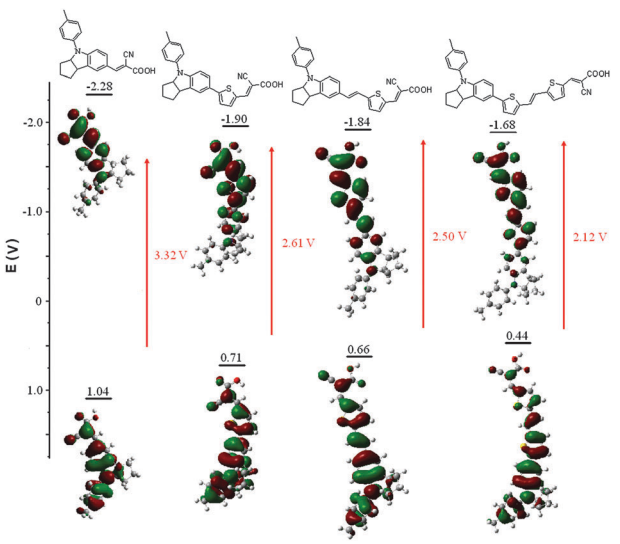

Fig. 2 Calculated HOMO and LUMO for **I-1**–**I-4**.

Table 3 Calculated TDDFT excitation energies for the lowest transition (eV, nm), oscillator strengths (*f*) and experimental absorption maxima[a]

	E (eV, nm)	*f*	Exp. (eV, nm)
I-1	2.74 (452)	1.1517	2.83 (438)
I-2	2.43 (509)	0.7768	2.52 (492)
I-3	2.31 (537)	1.2936	2.46 (504)
I-4	1.98 (626)	1.0996	2.39 (518)

[a] TDDFT excited state calculation was performed at the B3LYP/6-31G* level in vacuum with the B3LYP/6-31G* optimized ground-state geometry.

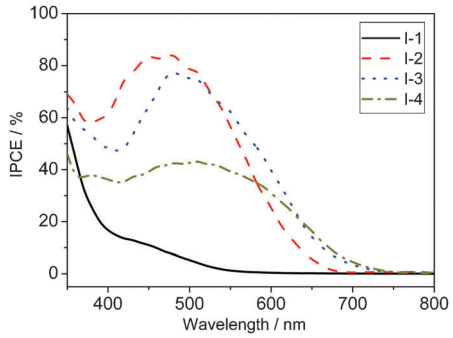

Fig. 3 IPCE action spectra of **I-1**–**I-4** based on liquid electrolyte in the visible region.

To further elucidate the performance of DSSCs, we compared *I*–*V* curves of solar cells sensitized with **I-1**, **I-2**, **I-3**, and **I-4**, respectively. The results under illumination of AM 1.5 (100 mW cm^{-2}) simulated solar light were shown in Fig. 4 and summarized in Table 4. **I-3** showed the highest short-circuit current density (J_{sc}) (10.63 mA cm^{-2}). Except for **I-4**, the J_{sc} of **I-1**–**I-3** were increased from 4.63 mA cm^{-2} to 10.63 mA cm^{-2} as ε was enhanced from 12 200 M^{-1} cm^{-1} to 41 500 M^{-1} cm^{-1}. Single molecule **I-4** possessed the highest light capture capability (48 600 M^{-1} cm^{-1}), but the amount of **I-4** adsorbed on TiO_2 electrode was the lowest one (Table 1) due to its relatively large molecular volume. Therefore, the J_{sc} of **I-4** was only 6.43 mA cm^{-2}, which was lower than **I-2** and **I-3**.

For **I-2**–**I-4**, the open-circuit voltage (V_{oc}) reduced from 725 mV to 632 mV when the π-conjugated linker of the dyes expanded. Compared with **I-2**, the sharp decrease of V_{oc} of **I-3** from 725 mV to 651 mV can be explained based on the

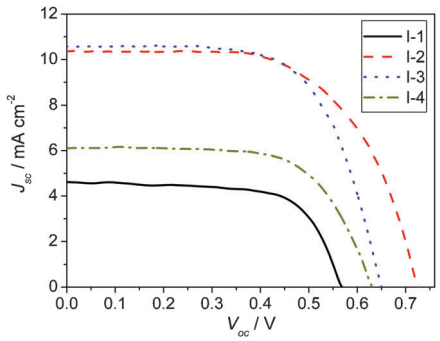

Fig. 4 *I*–*V* characteristics measured under an irradiance of 100 mW cm^{-2} (AM 1.5G).

Table 4 Photovoltaic performance of DSSCs based on **I-1**–**I-4** with liquid electrolyte

	J_{sc}/mA cm^{-2}	V_{oc}/mV	Fill factor	Efficiency, η (%)
I-1	4.63	568	0.67	1.79
I-2	10.38	725	0.62	4.58
I-3	10.63	651	0.64	4.46
I-4	6.43	632	0.65	2.53

theoretical calculations analysis, which is origin-dependent for charged species.[24] Generally, the V_{oc} is dependent upon the difference between the CB energy level of TiO_2 and the redox potential of the HTM. Thus, a CB energy level upshift is necessary to enhance photovoltage. Moreover, the dark-current generated from the recombination of electrons also has a great effect on the open-circuit photovoltage. Grätzel and coworkers found that larger dipole moment along the direction from sensitizer to TiO_2 (vertical) could suppress the dark current more effectively, thus resulting in an increase in open circuit voltage.[25] A favorable dipole moment of sensitizer can upshift the CB energy level efficiently. The dipole moments of **I-2** and **I-3** at their optimized geometry were calculated by hybrid density functional theory (B3LYP) with the 6-31G* basis set as implemented in the Gaussian 03 program[22] and listed in Table 4. As shown in Fig. 5, the *z*-axis extends out of the plane of the page and the TiO_2 surface plane is parallel to the *y*- and *z*-axes. Considering their bidentate binding mode, the dye molecules are positioned in such a way that the C_2 axis of the carboxylate is parallel to the *x*-axis. Therefore, their orientations after anchoring on to the TiO_2 are simulated. The components of dipoles parallel to the *z*-axis are fixed at zero.[26]

The vertical component of dipoles (*x* components) of two sensitizers possess the same direction but with different magnitude (10.28 D and 7.07 D for **I-2** and **I-3**, respectively, Table 5). Once adsorbed on TiO_2, the larger dipole moment along the direction for **I-2** can lead to more negative charges located close to the TiO_2 surface than that of **I-3**, resulting in a larger CB energy level upshift.

Meanwhile, the adsorption angle θ was reduced from 50.20° to 35.68° when π system was expanded. Actually, the adsorption form will affect the interfacial charge recombination to a considerable extent, which is another major factor influencing photovoltage.[27] While the adsorption angle θ was reduced along with the expansion of the π system, the blocking moiety

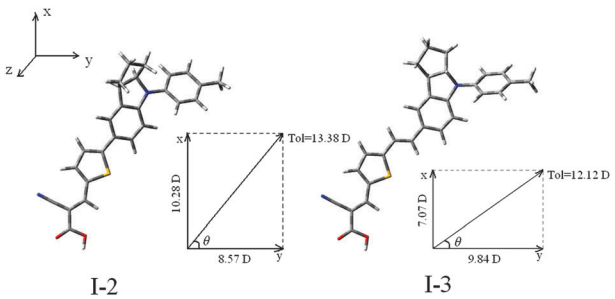

Fig. 5 Optimized geometrical structures and calculated total dipole moments of **I-2** and **I-3**.

Table 5 Calculated dipole components for **I-2** and **I-3**

	Dipole moments/D			
	x	*y*	Total	θ
I-2	10.28	8.57	13.38	50.20°
I-3	7.07	9.84	12.12	35.68°

(indoline group in these dyes) could not cover the π-linker segment and TiO_2 surface anymore and left them open to the electrolyte, which would cause charge recombination between I_3^- and excited electrons in the CB of TiO_2. Moreover, while the adsorption angle θ was reduced, the bound I_3^- would be brought very close to TiO_2 by the low-lying binding site, which would also cause this interfacial charge recombination.[26,28–30] Therefore, the charge recombination dynamic can be adjusted through optimizing the anchoring form which could be realized by modifying chemical structures of sensitizers.

Comprehensively, the more favorable dipole moment and adsorption form of **I-2** led to a larger CB energy level upshift and more effective suppression of charge recombination, which in turn results in a higher open-circuit photovoltage than **I-3**.

Interestingly, the above disciplines for indoline series dyes were different from the trends of triphenylamine dyes reported by Liang *et al.*,[26] which was caused by the characteristic of a certain system (indoline-thiophen in this work). Just for this reason, in order to design and synthesize sensitizer with high photovoltaic performance, an independent optimization through molecular engineering is doubtlessly necessary.

Overall, DSSCs based on liquid electrolyte sensitized by **I-2** and **I-3** produced similar results, with J_{sc} of 10.40 and 10.63 mA cm^{-2}, V_{oc} of 725 and 651 mV, *ff* of 0.62 and 0.64 and efficiency η of 4.58% and 4.46%, respectively. Under the same conditions, **I-4** only produced an overall conversion efficiency of 2.53% due to its relatively low amount of adsorbed dyes on TiO_2.

Also, we have tested the photovoltaic performance of quasi-solid state DSSCs using ionic liquid electrolyte consisting of BMII/I_2/BI/GuSCN (w/w, 40/1.67/0.67/3.33) and the results are listed in Table 6. The IPCE action spectra of quasi-solid state DSSCs were quite similar with those based on liquid electrolyte (Fig. 6). From 400–600 nm, **I-2** possessed higher IPCE values than the others and reached a maximum value of 81% at 480 nm. Remarkably, there was no obvious reduction of photocurrent for **I-2** compared with liquid electrolyte based devices (9.39 *vs.* 10.38 mA cm^{-2}), which means that the dilemma between optical absorption and charge diffusion lengths can be balanced through rational molecular engineering of organic sensitizers.[31]

Table 6 Photovoltaic performance of DSSCs based on **I-1**–**I-4** with ionic liquid electrolyte

	J_{sc}/mA cm^{-2}	V_{oc}/mV	*ff*	η (%)
I-1	3.07	552	0.61	1.04
I-2	9.39	698	0.51	3.37
I-3	7.76	640	0.51	2.38
I-4	6.13	630	0.56	2.34

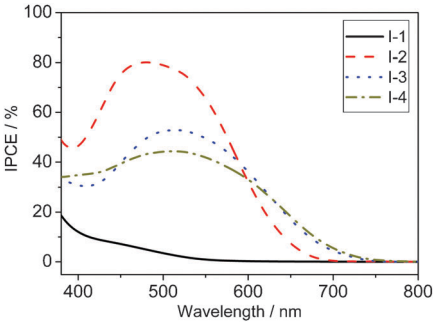

Fig. 6 IPCE action spectra of **I-1**–**I-4** based on ionic liquid electrolyte.

Conclusion

In summary, novel indoline dyes, **I-1**–**I-4**, with structural modification of π-linker group in the D-π-A system have been synthesized and fully characterized. The photophysical, electrochemical, and photovoltaic properties of the dyes were tuned efficiently. The ground and excited state properties of the dyes have been studied by the means of density functional theory (DFT) and time-dependent DFT (TD-DFT). The larger π-conjugation linker would lead to broader spectral response and higher molar extinction coefficient but decrease dye-loaded amount on TiO_2 electrode and LUMO level. The variation trends in J_{sc} and V_{oc} were observed to be opposite to each other. The internal reasons were studied by experimental data and theoretical calculations in detail. Beside liquid electrolyte based devices, quasi-solid state devices based on ionic electrolyte have been fabricated. Notably, **I-2** showed comparable photocurrent values based on these two devices (10.38 and 9.39 mA cm^{-2} for liquid and quasi-solid state electrolyte, respectively), which suggested through molecular engineering of organic sensitizers the dilemma between optical absorption and charge diffusion lengths can be balanced well. Through studies of photophysical, electrochemical, and theoretical calculation results, the internal relations between chemical structure and efficiency have been revealed, which serve to enhance our knowledge regarding design and optimization of new sensitizers for quasi-solid state DSSCs, providing a powerful strategy for prediction of photovoltaic performances.

Acknowledgements

This work was supported by Science Foundation of Hebei Normal University (L2009B08) and the Nature Science Foundation of Hebei Province (B2010000372).

Notes and references

1 B. O'Regan and M. Grätzel, *Nature*, 1991, **353**, 737.
2 M. Pagliaro, G. Palmisano, R. Ciriminna and V. Loddo, *Energy Environ. Sci.*, 2009, **2**, 838.
3 A. Hagfeldt, G. Boschloo, L. Sun, L. Kloo and H. Pettersson, *Chem. Rev.*, 2010, **110**, 6595.
4 Md. K. Nazeeruddin, A. Kay, I. Rodicio, R. Humphry-Baker, E. Mueller, P. Liska, N. Vlachopoulos and M. Grätzel, *J. Am. Chem. Soc.*, 1993, **115**, 6382.
5 J. H. Yum, I. Jung, C. Baik, J. Ko, Md. K. Nazeeruddin and M. Grätzel, *Energy Environ. Sci.*, 2009, **2**, 100.
6 Md. K. Nazeeruddin, P. Pechy and M. Grätzel, *Chem. Commun.*, 1997, 1705.

7 P. Wang, S. M. Zakeeruddin, J. E. Moser, Md. K. Nazeeruddin, T. Sekiguchi and M. Grätzel, *Nat. Mater.*, 2003, **2**, 402.
8 P. Wang, C. Klein, R. Humphrey-Baker, S. M. Zakeeruddin and M. Grätzel, *J. Am. Chem. Soc.*, 2005, **127**, 808.
9 T. Horiuchi, H. Miuraa and S. Uchida, *Chem. Commun.*, 2003, 3036.
10 S. Ito, S. M. Zakeeruddin, R. Humphry-Baker, P. Liska, R. Charvet, P. Comte, Md. K. Nazeeruddin, P. Péchy, M. Takata, H. Miura, S. Uchida and M. Grätzel, *Adv. Mater.*, 2006, **18**, 1202.
11 B. Liu, W. H. Zhu, Q. Zhang, M. Xu, Z. Ning, Y. Xie and H. Tian, *Chem. Commun.*, 2009, 1766.
12 T. Le Bahers, T. Pauporte, G. Scalmani, C. Adamo and I. Ciofini, *Phys. Chem. Chem. Phys.*, 2009, **11**, 11276.
13 D. Kim, J. K. Lee, S. O. Kang and J. Ko, *Tetrahedron*, 2007, **63**, 1913.
14 D. P. Hagberg, T. Marinado, K. M. Karlsson, K. Nonomura, P. Qin, G. Boschloo, T. Brinck, A. Hagfeldt and L.-C. Sun, *J. Org. Chem.*, 2007, **72**, 9550.
15 T. Marinado, D. P. Hagberg, M. Hedlund, T. Edvinsson, E. M. J. Johansson, G. Boschloo, H. Rensmo, T. Brinck, L.-C. Sun and A. Hagfeldty, *Phys. Chem. Chem. Phys.*, 2009, **11**, 133.
16 H. Choi, I. Raabe, D. Kim, F. Teocoli, C. Kim, K. Song, J.-H. Yum, J. Ko, Md. K. Nazeeruddin and M. Grätzel, *Chem.–Eur. J.*, 2010, **16**, 1193.
17 J. Tang, J. L. Hua, W. J. Wu, J. Li, Z. G. Jin, Y. T. Long and H. Tian, *Energy Environ. Sci.*, 2010, **3**, 1736.
18 K. Hara, Z. S. Wang, T. Sato, A. Furube, R. Katoh, H. Sugihara, Y. Dan-oh, C. Kasada, A. Shinpo and S. Suga, *J. Phys. Chem. B*, 2005, **109**, 15476.
19 Z. S. Wang, Y. Cui, K. Hara, Y. Dan-Oh, C. Kasada and A. Shinpo, *Adv. Mater.*, 2007, **19**, 1138.
20 L. Y. Luo, C. J. Lin, C. S. Hung, C. F. Lo, C. Y. Lin and E. W. G. Diau, *Phys. Chem. Chem. Phys.*, 2010, **12**, 12973.
21 S. Roquet, A. Cravino, P. Leriche, O. Alévêque, P. Frère and J. Roncali, *J. Am. Chem. Soc.*, 2006, **128**, 3459.
22 M. J. Frisch, G. W. Trucks, H. B. Schlegel, G. E. Scuseria, M. A. Robb, J. R. Cheeseman, J. A. Montgomery, Jr., T. Vreven, K. N. Kudin, J. C. Burant, J. M. Millam, S. S. Iyengar, J. Tomasi, V. Barone, B. Mennucci, M. Cossi, G. Scalmani, N. Rega, G. A. Petersson, H. Nakatsuji, M. Hada, M. Ehara, K. Toyota, R. Fukuda, J. Hasegawa, M. Ishida, T. Nakajima, Y. Honda, O. Kitao, H. Nakai, M. Klene, X. Li, J. E. Knox, H. P. Hratchian, J. B. Cross, V. Bakken, C. Adamo, J. Jaramillo, R. Gomperts, R. E. Stratmann, O. Yazyev, A. J. Austin, R. Cammi, C. Pomelli, J. Ochterski, P. Y. Ayala, K. Morokuma, G. A. Voth, P. Salvador, J. J. Dannenberg, V. G. Zakrzewski, S. Dapprich, A. D. Daniels, M. C. Strain, O. Farkas, D. K. Malick, A. D. Rabuck, K. Raghavachari, J. B. Foresman, J. V. Ortiz, Q. Cui, A. G. Baboul, S. Clifford, J. Cioslowski, B. B. Stefanov, G. Liu, A. Liashenko, P. Piskorz, I. Komaromi, R. L. Martin, D. J. Fox, T. Keith, M. A. Al-Laham, C. Y. Peng, A. Nanayakkara, M. Challacombe, P. M. W. Gill, B. G. Johnson, W. Chen, M. W. Wong, C. Gonzalez and J. A. Pople, *GAUSSIAN 03 (Revision C.01)*, Gaussian, Inc., Wallingford, CT, 2004.
23 A. Dreuw and M. Head-Gordon, *J. Am. Chem. Soc.*, 2004, **126**, 4007.
24 P. Chen, J. H. Yum, F. De Angelis, E. Mosconi, S. Fantacci, S. J. Moon, R. Humphry Baker, J. Ko, Md. K. Nazeeruddin and M. Grätzel, *Nano Lett.*, 2009, **9**, 2487.
25 J. Krüger, U. Bach and M. Grätzel, *Adv. Mater.*, 2000, **12**, 447.
26 Y. L. Liang, B. Peng and J. Chen, *J. Phys. Chem. C*, 2010, **114**, 10992.
27 B. A. Gregg, F. Pichot and S. Ferrere, *J. Phys. Chem. B*, 2001, **105**, 1422.
28 A. Burke, S. Ito, H. Snaith, U. Bach, J. Kwiatkowski and M. Gratzel, *Nano Lett.*, 2008, **8**, 977.
29 Z. S. Wang and G. Zhou, *J. Phys. Chem. C*, 2009, **113**, 15417.
30 D. P. Hagberg, J.-H. Yum, H. Lee, F. De Angelis, T. Marinado, K. M. Karlsson, R. Humphry-Baker, L. Sun, A. Hagfeldt, M. Grätzel and Md. K. Nazeeruddin, *J. Am. Chem. Soc.*, 2008, **130**, 6259.
31 H. Qin, S. Wenger, M. Xu, F. Gao, X. Jing, P. Wang, S. M. Zakeeruddin and M. Grätzel, *J. Am. Chem. Soc.*, 2008, **130**, 9202.

